nature communications

Article

https://doi.org/10.1038/s41467-025-60829-8

Amino acid transporters mediate autonomous delivery of nanoparticle vehicles into living plants

Received: 17 January 2024

Accepted: 4 June 2025

Published online: 21 July 2025

Check for updates

Xue Xia[1,2,3,8], Jiawei Dong[1,2,8], Aijie Li[1,2,8], Yanlin Wang[1,2], Yang Liu[1,2], Yingfang Zhu[3], Liang Xu[1,2], Zhiyang Jing[1,2], Jing Wang[1,2], Yan Zou[1,2,4], Shiyong Sun[3], Lu Wang[5], Yiqing Lu[1,6], Alex Soeriyadi[7], Xuelu Wang[3], John W. Patrick[5], Christina E. Offler[5], Meng Zheng[1,2] ✉, Chun-Peng Song[3] ✉ & Bingyang Shi[1,4] ✉

Presence of the cell wall and the lack of streamlined pathways for cellular delivery of external agents into plants is a core challenge of plant biotechnology and crop engineering development. However, both viral and bacterial transmission have their own restrictions and the few non-heavy metal nanodelivery platforms require external forces for tissue penetration. Such dependency limits any high-throughput application considering the large plant numbers to be treated in the field or even laboratory exercises. Herein, we demonstrate Aspartic acid (Asp) decorated poly(ethylene glycol)-block-poly(2-(diisopropylamino)ethyl methacrylate) (Asp-PEG-PDPA) copolymers assembled micelles (Asp/PDPA-NP), a platform that utilises amino acid transporters (AtAAP1 and AtLHT1) as receptors for clathrin-dependent endocytosis, freely translocate to release loaded cargo into various plant tissue/cell types in a species-independent manner within ≤10 minutes through simple spray or co-culture. As proof-of-concept, abscisic acid (ABA)-loaded Asp/PDPA-NP was tested for its efficacy to confer plant drought resistance. Asp/PDPA-NP@ABA reduced the effective ABA dose down to 1 nM (one million-fold) and elicited anti-drought potency in representative eudicot (soybean) and monocot (maize) crop species. Owing to its delivery efficiency, Asp/PDPA-NP holds promise as a potent carrier for diverse chemicals and biomolecules in plant systems.

Delivering exogenous agents (imaging probes, chemical drugs and genetic engineering tools) into biological systems to effect their in vivo response is key to biotechnology development[1–3]. Generally, biotechnologists incorporate those agents into bacteria and viruses for *in planta* delivery however, their practices are still challenged by high cost, the lack of efficiency or species limitations[4].

Since the 1990s[5], a new transportation route by nanomaterials with a versatile targeting capacity and protection of their cargoes[3], has

[1]The Zhongzhou Laboratory for Integrative Biology, Henan-Macquarie University Joint Centre for Biomedical Innovation, School of Life Sciences, Henan University, Kaifeng, China. [2]Henan Key Laboratory of Brain Targeted Bio-nanomedicine, School of Life Sciences & School of Pharmacy, Henan University, Kaifeng, China. [3]State Key Laboratory of Crop Stress Adaptation and Improvement, School of Life Sciences, Henan University, Kaifeng, China. [4]School of Biomedical Engineering, University of Technology Sydney, Sydney, NSW, Australia. [5]School of Environmental and Life Sciences, College of Engineering, Science and Environment, University of Newcastle, Callaghan, NSW, Australia. [6]School of Engineering, Macquarie University, Sydney, NSW, Australia. [7]Agnetic Bio Innovation, Eveleigh, NSW, Australia. [8]These authors contributed equally: Xue Xia, Jiawei Dong, Aijie Li. ✉e-mail: mzheng@henu.edu.cn; songcp@henu.edu.cn; bs@henu.edu.cn

resulted in successful clinical therapeutic applications. In contrast, delivery of exogenous agents for plant biotechnological purposes lags behind. Major barriers are the plant cell wall, a cellulose and hemicellulose framework embedded within a cushion of pectin[6] with an exclusion limit of less than 5 nm[7], and the plasma membrane. Emerging studies suggest that physiochemical properties of nanoparticles, including size[8], shape[9], surface charges[10] could affect their entry into plants. Yet, for the current published arsenal of nanovehicles to breach the cell wall and plasma membrane depends on either spraying rather small sized (less than 5 nm in diameter) nanoparticles[11,12], or mechanical force[9,13,14]. A few other targeted delivery studies tried biorecognitions decoration[12,15] to facilitate their entry. Thus, a heavy-metal free, non-toxic and highly efficient nanodelivery vehicle, that requires no external force for entry, would provide a breakthrough tool to expedite plant biotechnology, sustainable agriculture and food security.

To this end, we focused on developing a delivery system that can efficiently translocate cargoes, in the absence of external forces, across both the cell wall and plasma membrane into various plant cell types across different plant species. For plasma membrane passage, biomedical studies have demonstrated the ability of amino acid transporters to mediate the uptake of L-amino acid decorated nano-scale particles[16,17]. Based on this evidence, we hypothesised plant amino acid transporters could mediate nanocarriers using their universally transported molecule, aspartic acid (Asp)[18–20], as their binding ligand. To test this approach, an autonomous delivery system (Asp/PDPA-NP) was self-assembled from Asp decorated poly(ethylene glycol)-block-poly(2-(diisopropylamino)ethyl methacrylate) (Asp-PEG-PDPA) copolymers. The Asp/PDPA-NP vehicle accomplished fast and efficient delivery across both the cell wall and the plasma membrane in various tissue/cell types of diverse plant species via a simple spray or co-culture application. Cell wall permeability was found to be increased by the polymer while plasma membrane passage resulted from clathrin-dependent endocytosis of amino acid transporter (AtAAP1 and AtLHT1)/vehicle complex.

Using abscisic acid (ABA) as a model cargo, the translational potential of the Asp/PDPA-NP system "from benchtop to the field" was demonstrated by a single spray of Asp/PDPA-NP@ABA, significantly prolonging plant resistance to water deprivation. This phenomenon was observed in Arabidopsis, as well as soybean (*Glycine max*) and maize (*Zea mays*). The ease of application and high uptake efficiency may allow its large-scale translation to agricultural applications such as broadacre cropping.

Results

Autonomous translocation of Asp/PDPA-NP into plant cells

Asp-PEG-PDPA was synthesised (Supplementary method) from hydroxy-PEG-ω−4-cyanopentanoic acid dithionaphthalenoate (HO-PEG-CPADN), followed by reversible addition-fragmentation chain transfer polymerization with 2-(diisopropylamino)ethyl methacrylate (DPA) and conjugation with α-aspartic acid (Asp). H^1NMR demonstrated the successful synthesis of Asp-PEG-PDPA (Supplementary Fig. 1). Asp/PDPA-NP was constructed through self-assembly (Fig. 1a, b), and its core maintains the capacity of loading designated agent(s).

To verify if Asp/PDPA-NP can be loaded into plant cells, we first employed DiO (3,3′-dioctadecyloxacarbocyanin) as a membrane-impermeant fluorescent tracer. Here DiO was loaded, through self-assembly, into the hydrophobic region of the micelle to form Asp/PDPA-NP@DiO with a mean diameter of 166.1 ± 3.5 nm, polydispersity index (PDI) at 0.154 ± 0.03, relatively positively charged (Supplementary Fig. 5b–e) and an average drug loading efficiency (DLE) of 65.1% (Supplementary Table S2). For each experiment, amounts of DiO loaded into Asp/PDPA-NP or PDPA-NP were calibrated to be identical to the applied pristine DiO. The Asp/PDPA-NP@DiO micelles were topically sprayed onto Arabidopsis leaves and then washed before viewed in transverse (Fig. 1d) and longitudinal (Fig. 1e) sections by confocal microscopy (see cartoon illustration in Fig. 1c). Asp transporters likely facilitate the uptake of Asp-decorated nanoparticles into leaf mesophyll cells[19–21]. AtAAP1 is predominantly localised in the root tips and epidermis cells[19,22], with some level of expression in source leaf mesophylls[23,24], while AtLHT1 shows strong expression in[21,24]. In transverse section, DiO fluorescence occurred across the entire depth of Arabidopsis leaves 12 h after exposure to Asp/PDPA-NP@DiO spray on their adaxial surfaces (Fig. 1d), demonstrating an efficient leaf tissue penetration. In longitudinal sections, DiO signal was observed in spongy mesophyll cells (Fig. 1e). We also revealed a colocalised signal between Asp/PDPA-NP delivered DiO fluorescence (green) and chloroplast autofluorescence (red) (Fig. 1f), with an averaged Pearson's colocalisation coefficient $r = 0.60 \pm 0.02$ and a Manders' correlation coefficient of 0.93 ± 0.00, suggesting a higher protoplasmic internalisation of DiO delivered by Asp/PDPA-NP.

Internalisation across the plasma membrane was further confirmed by culturing isolated protoplasts in media containing Asp/PDPA-NP@DiO. Here membrane impermeable DiO and PDPA-NP@DiO groups only exhibited signal on the plasma membrane. In contrast, intense fluorescence was observed intracellularly for protoplasts cultured in Asp/PDPA-NP@DiO (Supplementary Fig. 2), confirming Asp/PDPA-NP's ability to transverse the plasma membrane.

Asp/PDPA-NPs transverse into multiple tissue/cell types of differing plant species

A technique that universally applies to all tissue/cell types in a species-independent manner is most desirable for application in plant biotechnology. To test this proposition, the high transverse efficacy of topically applied Asp/PDPA-NP observed for Arabidopsis leaves (Fig. 1) was further evaluated in leaves, roots and seeds across a selection of other monocot (maize and tradescantia) and eudicot (soybean) species.

Protoplasmic entry of topically applied Asp/PDPA-NP@DiO could be demonstrated for leaf subepidermal and mesophyll cells of maize longitudinal sections (Fig. 2a). In the case of tradescantia, the absence of stomata[25] on the adaxial leaf surface suggests that the uptake of Asp/PDPA-NP@DiO into its adaxial epidermis (Fig. 2a) is via a non-stomatal apoplasmic route. Thus, as no surface surfactant was employed, Asp/PDPA-NP must have facilitated transfer across the hydrophobic cuticle layer of tradescantia.

In relation to biotechnological application to crops, supply of cargos to roots is also of great importance. Autonomous uptake was evaluated in roots of Arabidopsis, maize (Fig. 2b) and soybean (Supplementary Fig. 3) cultured hydroponically with Asp/PDPA-NP. Arabidopsis and maize seedling roots exposed to culture media containing Asp/PDPA-NP@DiO showed significantly more intracellular signal than any other treatment.

To further confirm the above observation, by tagging the hydrophobic region of the nanoparticle with fluorescein isothiocyanate (FITC), we have also performed z-stack and time-lapse tracing of micelles themselves rather than its cargo after foliar and root application in tradescantia leaf, maize and soybean roots (Supplementary Fig. 3). Significantly higher uptake of Asp/PDPA-NP-FITC was observed in tradescantia leaves down to > 40 μm beneath the sprayed adaxial epidermis (Supplementary Fig. 3a). Similar findings of DiO-loaded nanoparticles (Fig. 2b) applied to Asp/PDPA-NP-FITC entering into roots of maize and soybean seedlings (Supplementary Fig. 3b, c). Z-stack tracing showed ample amount of Asp/PDPA-NP-FITC 50 μm into the root tissue, and builds up across time (Supplementary Fig. 3b, c). Entry of Asp-decorated micelles are also efficient, as time-tracing observation showed signal of Asp/PDPA-NP-FITC in cultured Arabidopsis roots epidermis within 10 min of exposure. Within 2 h, radial inward movement of FITC signal commenced and after 6 h, substantial FITC signal was observed at a depth of > 100 μm (Supplementary Fig. 4 and Supplementary Movie 1).

https://doi.org/10.1038/s41467-025-60829-8

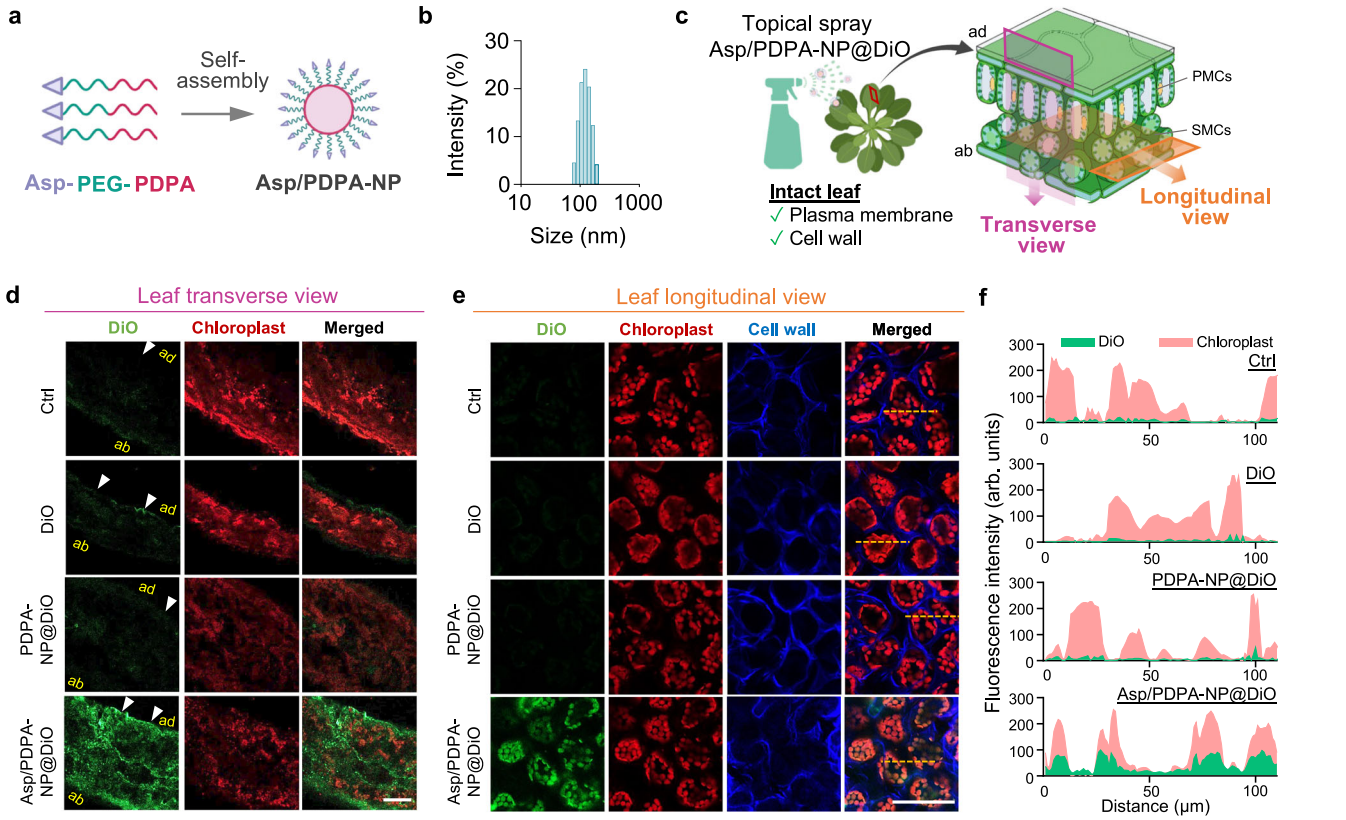

Fig. 1 | Asp/PDPA-NP efficient translocation at *in planta* and cellular levels. **a** Schematic illustration of Asp-PEG-PDPA self-assembly into micelles. Created in BioRender. Shi, B. (2025) BioRender.com/l4iah3l. **b** Particle size distribution of Asp/PDPA-NP. **c** Cartoon illustrating an Arabidopsis with its adaxial (ad) leaf surfaces topically sprayed with Asp/PDPA-NP@DiO and observed by confocal microscopy. Created in BioRender. Shi, B. (2025) BioRender.com/ngjlual. **d** Representative transverse view through adaxial (ad, white arrowheads) to the abaxial leaf epidermis (ab) or (**e**) longitudinal view into spongy mesophyll cells (SMCs) located below the ad leaf epidermis and palisade mesophyll cells (PMCs). Bar = 50 μm in (**d** and **e**). Green fluorescence: DiO signal; red fluorescence: chloroplast autofluorescence; blue fluorescence: cell wall stained with Calcofluor White ($n = 3$). White arrowheads indicate the adaxial epidermis where the spray was applied to. **f** Co-localisation analysis of leaf mesophyll chloroplast autofluorescence signal (pink) and nanoparticle delivered DiO signal (green) across the yellow dashed lines in (**e**). Source data are provided as a Source Data file.

The thick tissue compactness of the seed prevented the determination of intracellular localisation by microscopical observation of Asp/PDPA-NP@DiO. To overcome this impasse, we relied on testing the intracellular delivery of ABA that slows down seed germination through the PYR/PYL/RCAR–PP2C–SnRKs signalling cascade within the cytoplasmic compartment[26,27]. Brownian Movement[28,29] could provide the driving force for vehicle uptake in seeds. ABA was loaded into micelles through self-assembly to form Asp/PDPA-NP@ABA (Supplementary Fig. 5a) with a mean diameter and PDI of 134.3 ± 2.3 nm and 0.16 ± 0.04, respectively (Supplementary Fig. 5b–e) and positively charged (Supplementary Fig. 5e). High-performance liquid chromatography (HPLC) assays demonstrated an averaged 71.2 ± 1.9% DLE (Supplementary Table S2) for ABA, and marginal level of its loaded ABA are released by 1 h and then increased to less than 40% by 9 h under the pH of early endosome/trans-Golgi network and multivesicular body[30,31]. The release then turned into a slower process up to 72 h when 80% of ABA are released (Supplementary Fig. 5f). In this study, different concentrations of Asp/PDPA-NP@ABA were prepared for each assay. Based on their DLE (Supplementary Table S2), the amount of ABA loaded in Asp/PDPA-NP was calibrated identical to the pristine ABA level used in each experiment.

Arabidopsis seeds cultured in the presence of Asp/PDPA-NP@ABA exhibited a threefold slower germination than other treatments (Fig. 2c). This effect was ABA concentration-dependent and was still observable at 0.1 μM ABA (Supplementary Fig. 5h). The same compromised germination phenotype was also demonstrated for maize (Fig. 2c).

Asp/PDPA-NPs remodel the cell wall and traverse the plasma membrane via Asp transporters mediated endocytosis

Next, the mechanisms by which Asp/PDPA-NP enters plant cells were explored. In particular, the question raised from findings reported thus far is how do our nanoparticles, sized over 100 nm (Supplementary Fig. 5b), move across the densely packed cell wall and then through the plasma membrane?

Exposure of plasmolyzed cells of onion scale epidermis to the PDPA-NP delivered DiO signal led to it being primarily located outside the shrinking protoplasm in the cell wall and intercellular space. In contrast, the Asp/PDPA-NP shipped DiO was additionally located in the protoplasm (Fig. 3a, b). Matching fluorescent intensities in the apoplasm of both treatments suggest that PDPA-NP part of the micelle may induce a change in cell wall permeability (Fig. 3b). In addition, the transcriptome profile of Arabidopsis mature leaves exposed to PDPA-NP indicated a significant number of cell wall remodelling genes were induced (Fig. 3c).

Together, the above comparisons between Asp-decorated and non-decorated vehicles, confirmed that cell wall remodelling could be induced by PDPA-NP. However, the fast cellular uptake (≤ 10 min; Supplementary Fig. 4) of Asp/PDPA-NP led us to speculate that cell wall remodelling may initially be induced by a yet to-be-discovered post-translational regulatory mechanism. Indeed, the time-lapse study strongly corresponds with that for transient post-translational activation of rapid cell expansion by auxin[32].

Amino acid transporters that mediate Asp belong to several families. These include Amino Acid Permeases (AAP), Lysine/Histidine-

https://doi.org/10.1038/s41467-025-60829-8

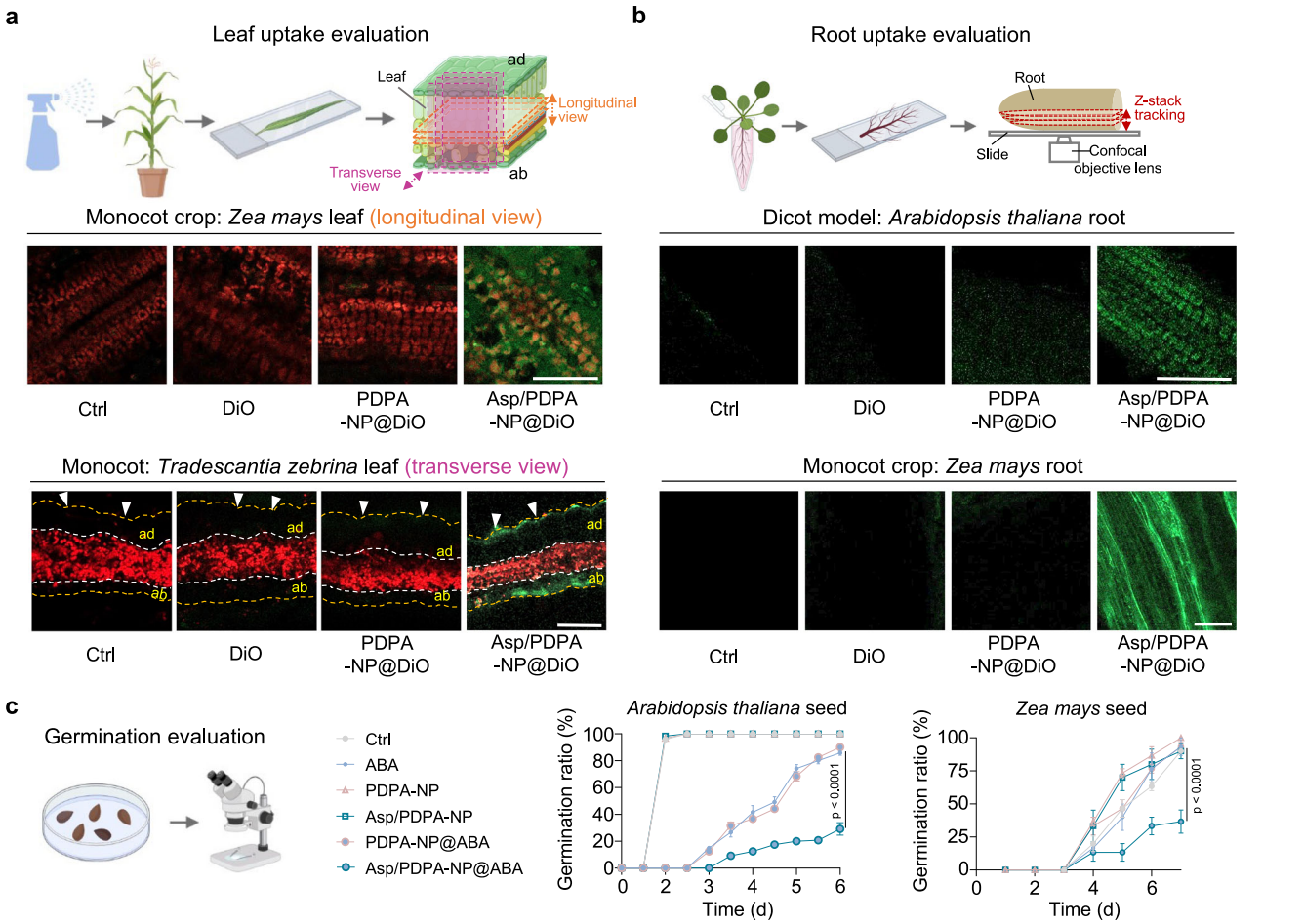

Fig. 2 | Asp/PDPA-NP intracellularly translocated into various tissue/cell types in a range of plant species. a Uptake of Asp/PDPA-NP@DiO post adaxial (ad) surface spray observed in subepidermal spongy mesophyll cells (maize) and adaxial and abaxial epidermis (tradescantia) of mature leaves. Bar = 100 µm. White arrow heads indicate the sprayed adaxial surface of the leaf. ab: abaxial surface. Green fluorescence: DiO signal; red fluorescence: chloroplast autofluorescence. Each treatment was tested in 3 biological replicates. **b** Asp/PDPA-NP@DiO loaded into *Arabidopsis thaliana* and *Zea mays* seedling roots in hydroponic culture conditions and visualised after 6 h at 40 µm underneath the epidermis. Green fluorescence: DiO signal. Bar = 100 µm. Each treatment was observed in 3 biological replicates. Created in BioRender. Shi, B. (2025) BioRender.com/orcsbbf. **c** Asp/PDPA-NP@ABA slows Arabidopsis and maize seed germination in comparison to other treatments. ABA concentration and equivalent ABA concentration in (Asp/)PDPA-NP@ABA is 0.5 and 50 µM for Arabidopsis and maize, respectively. Data are presented as mean values ± SEM. Each treatment was tested in 6 replicates of 20 seeds per replicate. Significant differences were determined using Turkey's one-way multiple comparison ANOVA test, the *P* value are as per noted. Created in BioRender. Shi, B. (2025) BioRender.com/wx4qesq. Source data are provided as a Source Data file.

type Transporters (LHT) and Proline/compatible solute Transporters (ProT)[18]. Due to the lack of specific inhibitors that target these transporters, a series of commercially available Arabidopsis mutants of amino acid transporters were used to identify those mediating Asp/PDPA-NP transport (Fig. 3d). Enhanced drought resistance induced by ABA[33,34] delivery, via Asp/PDPA-NP, was used as the phenotypic indicator for increased intracellular uptake of the nanoparticle vehicle and release of its cargo.

Screening the amino acid transporter mutants exposed to the various treatments demonstrated that elevated drought resistance conferred by Asp/PDPA-NP@ABA exposure was only absent from the *aap1* and *lht1* mutants (Fig. 3d). This suggests that these amino acid transporters are responsible for intracellular uptake of Asp/PDPA-NP across the plasma membrane; a conclusion further confirmed by the lack of upregulated expression of the cytosolic located ABA-responsive reporter gene, *Response to desiccation 29 A* (*RD29A*)[35] in *aap1* mutants, while normal upregulation were observed in *aap6* mutants and the wild-type plants after Asp/PDPA-NP@ABA treatment, respectively (Fig. 3e and Supplementary Fig. 6g).

The binding of AAP1 and LHT1 transporters with 100 nm diameter nanoparticles is more likely to immobilise the transporter proteins rather than mediate transmembrane crossing of the nanoparticle. An immobilised, and hence non-functional transporter, could well undergo endocytosis[36] as demonstrated in biorecognition-decorated nanoparticle uptake in mammalian cells[37]. Consistent with this proposition, a clathrin-mediated endocytosis inhibitor, tyrphostinA23 (Tyra23[38]), reduced intracellular uptake of Asp/PDPA-NP@DiO into Arabidopsis seedling roots (Fig. 3f). Thus, AAP1 and LHT1 may function as receptors to bind Asp-ligands and thereafter the complex is endocytosed facilitating shipping the cargo into the protoplasm in bulk (cartoon illustration in Fig. 3g).

Asp/PDPA-NP *in planta* functional efficiency can boost drought resistance

In the previous section, the Asp/PDPA-NP delivery system's ability to efficiently translocate and ship its cargo into living plant leaves via spray manner was demonstrated (Figs. 1 and 2). As a proof-of-concept for possible translation of the vehicle system into crop biotechnology, ABA-loaded Asp/PDPA-NP was used to test for its efficacy to confer plant drought resistance.

To this end, we explored the molecular events induced by spraying Arabidopsis with Asp/PDPA-NP@ABA. First, the leaf

https://doi.org/10.1038/s41467-025-60829-8

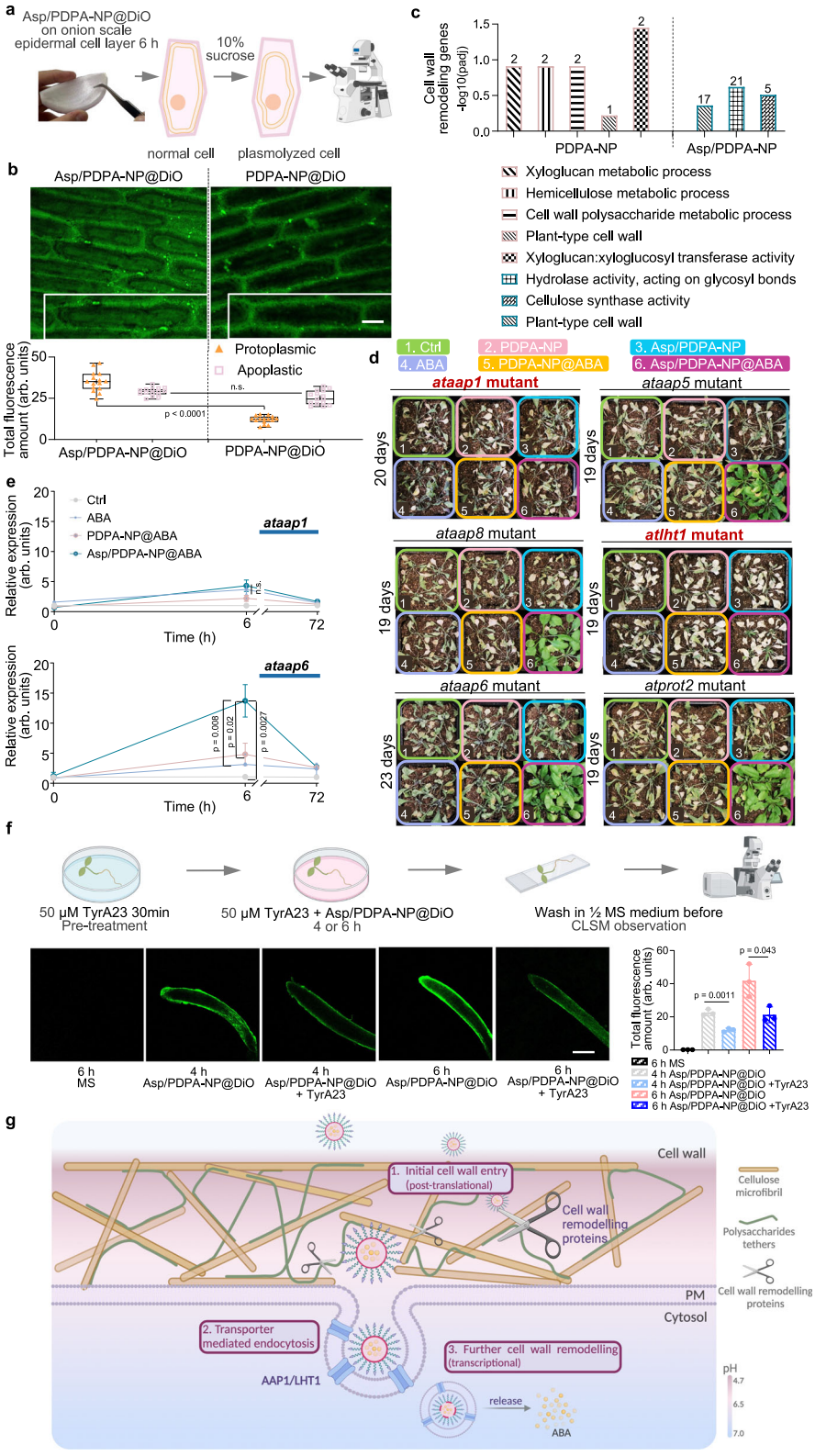

temperature changes detected in sprayed Arabidopsis plants (Supplementary Fig. 6a, b) demonstrate that the amount of ABA entering the protoplasm is sufficient to cause stomatal closure and reduce transpiration resulting in an increased leaf temperature[33,34].

In addition, 48 h post spray was chosen as large drought phenotypic effects were apparent at this time (Supplementary Fig. 6a, b). In total, 41 differentially expressed genes (DEGs) as ABA-related or -responsive between each treatment and their accompanying MS control were identified. Thirty ABA-related DEGs were upregulated 48 h post Asp/PDPA-NP@ABA spray (Supplementary Fig. 6c, d). These responses exceeded those induced by pristine ABA or PDPA-NP@ABA treatments (Supplementary Fig. 6c, d). Moreover, qPCR analyses of gene expression profiles across an entire 72 h post application were performed for the representative cytosolic-located ABA response marker genes, *Response to ABA 18* (*RAB18*[39]; Supplementary Fig. 6f; early response to ABA) and *RD29A*[35] (Supplementary Fig. 6g; late

Fig. 3 | Asp/PDPA-NP loosens the cell wall and enhances uptake by Asp transporters. a, **b** Cell wall or protoplasmic (**a**) distribution and (**b**) accompanying quantification of DiO signal delivered by PDPA-NP or Asp/PDPA-NP in onion scale epidermal cells after plasmolysis. Green fluorescence: DiO signal. Bar = 100 µm. Yellow: protoplasm; pink: apoplastic compartment. Total fluorescence of each cell was determined from Mean ± SEM of three biological replicates, measurement of 15 cells were determined for each replicate. Significant differences were determined using Turkey's one-way multiple comparison ANOVA test, the *P* value are as per noted. Data are presented as box-and-whisker plots in (**b**), where median and 25th and 75th percentiles are represented by the middle line and the box itself, respectively; means are indicated by a "+". Created in BioRender. Shi, B. (2025) BioRender.com/txwwnta. **c** GO analysed of differentially expressed genes identified as cell wall remodelling groups at 48 h post spray. Numbers mark the number of differentially expressed genes identified. The *y*-axis marks the significant change in the scale of the identified differentially expressed genes. **d** Asp/PDPA-NP@ABA enabled drought resistance are abolished in *ataap1* and *atlht1* mutants. Three-week-old mutant plants grown under short-day conditions were sprayed (~ 60 µL) with ½ MS medium (MS), 10 µM ABA, PDPA-NP or Asp/PDPA-NP loaded with/without an equivalent of 10 µM ABA. **e** qPCR analyses of expression profiles of *Response to desiccation 29 A* (*RD29A*) in *ataap1* and *ataap6* mutant plants at 0, 6 and 72 h post foliar spray ($n = 3$ biological replicates, each replicate is the total RNA extracted from 3 plants. Data are presented as mean values ± SEM. Significant differences were determined using Turkey's one-way multiple comparison ANOVA test, the *P* value are as per noted). **f** Tracking of Asp/PDPA-NP@DiO in Arabidopsis seedling root with/without clathrin inhibitor Tyra23 at 50 µM. Green fluorescence: DiO signal. Bar = 100 µm, $n = 3$ biological replicates. Data are presented as mean values ± SEM. Significant differences were determined using Student's two-tailed *t*-test, the *P* value are as per noted. Created in BioRender. Shi, B. (2025) BioRender.com/4464gbd. **g** Schematic illustration of the hypothesis of Asp/PDPA-NP sequentially loosening, and hence transporting within, the cell wall, followed by uptake across the plasma membrane via AAP1 or LHT1 transporter(s). Once within the protoplasm, Asp/PDPA-NP may upregulate expression of cell wall remodelling gene expression to positively feedback to further sustain cell wall loosening. Created in BioRender. Shi, B. (2025) BioRender.com/iz4jut6. Source data are provided as a Source Data file.

response to ABA). Their upregulation demonstrates a distinct enhancement by Asp/PDPA-NP@ABA in both early and late ABA-induced transcriptomic responses. Together, these findings suggested more ABA was transported by Asp/PDPA-NP intracellularly to induce the subsequent molecular event.

Arabidopsis seedlings sprayed with Asp/PDPA-NP@ABA showed significant anti-drought capacity in comparison to other treatments (Fig. 4a). This was reflected by plants sprayed with Asp/PDPA-NP@ABA having a twofold higher relative water content compared to any other treatment at day 8 post water withdrawal (Supplementary Fig. 6e). Multiple repeats of the experiment showed that a single spray of Asp/PDPA-NP@ABA (~ 60 µL at 10 µM per plant) extended longevity by 57% and secured a 100% survival rate[40] compared to other treatments (Fig. 4b, c; c calculated from plants treated in Supplementary Fig. 6i).

We then evaluated the efficiency by which Asp/PDPA-NP transports ABA across the cell wall and the plasma membrane. This was done by comparing ABA levels in the extracellular (i.e., cell wall, cuticle, middle lamella and the intercellular space) and protoplasmic compartments (Fig. 4d). Identical amounts of ABA were detected in the extracellular matrix of plants sprayed with PDPA-NP or Asp/PDPA-NP. These levels were 1.8-fold higher than those for the pristine ABA treatment (Fig. 4e). Notably, uptake of ABA from the extracellular matrix into protoplasm was substantially greater (39-fold) in plants sprayed with Asp/PDPA-NP@ABA than ABA alone (Fig. 4e). Overall, Asp/PDPA-NP boosted cargo delivery across the cell wall and plasma membrane by 69-fold comparing with pristine ABA.

The high cost of pristine ABA delivered as a crop spray prohibits its adoption as an agronomic strategy to confer drought resistance. Promisingly, the substantially higher efficacy of ABA delivery by Asp/PDPA-NP@ABA could bridge this impediment. To this end a comparative phenotypic dose-response study was undertaken between Arabidopsis plants sprayed with pristine ABA or Asp/PDPA-NP@ABA. The study found that drought resistance conferred by 10 µM to 1 mM ABA exhibited a concentration-dependent response. In contrast, Asp/PDPA-NP@ABA, across 1 nM to 1 µM, elicited a concentration-independent response identical to that conferred by 1 mM pristine ABA (Fig. 4f and Supplementary Fig. 6j, k) pointing to a 10^6 greater efficacy.

A further step in exploring the feasibility of using our vehicle in crop field conditions was demonstrated by nanovehicle protection of ABA from UV degradation (Supplementary Fig. 5g). More importantly, drought tolerance conferred by foliar spray of Asp/PDPA-NP@ABA was assessed using the significant crop species, soybean and maize.

As a result, leaf temperature was found to increase after spraying 15 d-old William 82 soybean plants at their three trifoliate stage (Supplementary Fig. 7a) when sprayed with 50 µM equivalent of ABA. The initial increase of leaf temperature 12 h after Asp/PDPA-NP@ABA spray (Supplementary Fig. 7a, b) suggests an effective translocation of ABA into the leaf protoplasm. Significantly, exposure to a single foliar spay of a lower ABA dose (10 µM) elicited a twofold increase in median survival length post water withdrawal (Fig. 4g, Supplementary Fig. 7c). Maize also exhibited an extended longevity to a single foliar spray with Asp/PDPA-NP@ABA at 50 µM (Supplementary Fig. 8). Together, these findings provided confidence for the technology's potential for use in field crops. This is particularly so for maize as a representative of the Poaceae family whose thick hydrophobic cuticles repel most sprays that can only be overcome by surface surfactants and high ABA concentrations.

Agronomic use of a polymeric nanocarrier to elevate crop drought resistance raises questions about its biocompatibility. In this context, the nanocarrier did not elicit cell/protoplast disfiguration or any non-ABA-induced plant/seed aberrant phenotypes (e.g., see Fig. 4a, f and h, and Supplementary Figs. 2, 6 and 7). Consistent with these observations was an absence of any significant expression response of the acute cytotoxicity reporter gene, Respiratory *b*urst *o*xidase *h*omologue B (*RbohB*)[9] up to 72 h post-application (Supplementary Fig. 6h).

Discussion

Our Asp/PDPA-NP vehicle breached the two most challenging hurdles for nanoparticle delivery systems facing plant biotechnology. That is, the densely packed cell wall and transfer across the plasma membrane. This was achieved by possibly rapid loosening of the cell wall and then utilising Asp transporters for transmembrane passage. As a consequence, the system avoids reliance on external aids that severely limit their utility in crop biotechnology.

To illustrate its biotechnological potency in plants, an Asp/PDPA-NP based anti-drought spray was developed to deliver ABA. This conferred ABA-mediated drought resistance in Arabidopsis, and representative crop species, soybean and maize, in the absence of any plant phenotypic effects. Most impressively, Asp/PDPA-NP@ABA enhanced ABA anti-drought efficacy by 10^6-fold. Another potential utility of the ABA delivery system is the inhibition of pre-harvest sprouting under high humidity conditions and reduced dormancy[41]. Similar comment applies to capturing ABA's ability to redirect nutrient flows into reproductive organs under drought[42] to enhance crop yield. Combined with ease of synthesis, high efficacy of cargo delivery, in vitro stability and simple spray-on application, these features of Asp/PDPA-NP@ABA point to its promising agronomic potential for large-scale field delivery. Most benefit will be realised in developing countries where such technologies are required to be economically accessible and readily disseminated[43]. However, further studies are required to assess field deployment. These include field trials as well as Asp/PDPA-NP *in planta* translocation,

https://doi.org/10.1038/s41467-025-60829-8

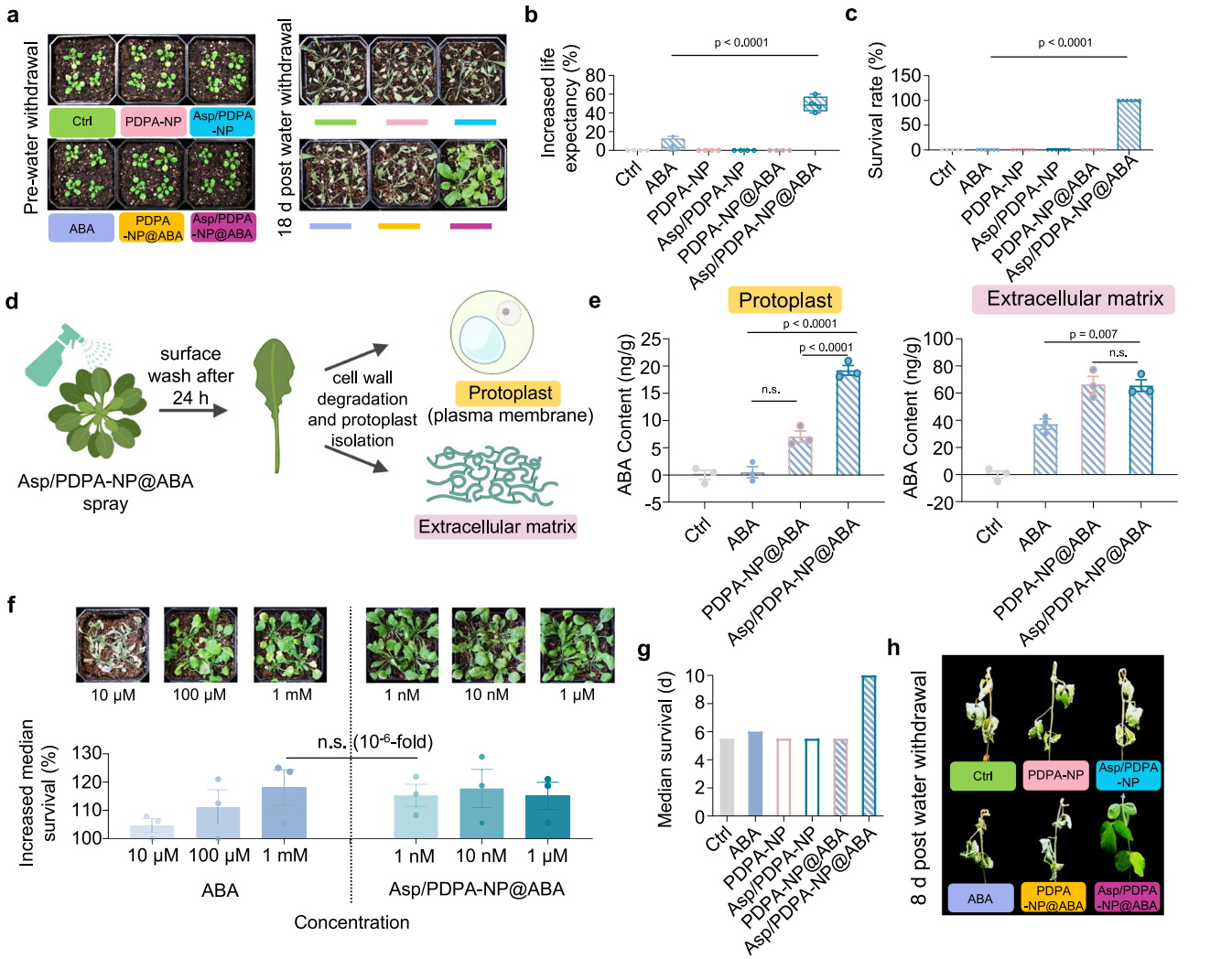

Fig. 4 | Asp/PDPA-NP *in planta* efficacy of conferring drought resistance in crop species. a Seventeen-day-old wild-type Arabidopsis plants (Col-0) grown under short-day conditions and sprayed (~60 µL) with ½ MS medium (MS), 10 µM ABA, PDPA-NP or Asp/PDPA-NP loaded with/without an equivalent of 10 µM ABA before water withdrawal; **b** Asp/PDPA-NP@ABA increased their longevity ratio and **c** survival rate, following 11 d water withdrawal + 2 d rewater. Data are presented as mean values ± SEM. $n = 8$ biological replicates. Significant differences were determined using Turkey's one-way multiple comparison ANOVA test, the P value are as per noted. Data are presented as box-and-whisker plots in (**b**), where median and 25th and 75th percentiles are represented by the middle line and, the box itself, respectively; means are indicated by a "+". **d** illustration and (**e**) quantitative ABA contents measured in protoplasmic versus extracellular matrix compartments extracted from Arabidopsis leaves sprayed with/without Asp/PDPA-NP@ABA after 24 h ($n = 3$ biological replicates, each replicate is the total amount of ABA collected from 48 plants. Data are presented as mean values ± SEM. Significant differences were determined using Turkey's one-way multiple comparison ANOVA test, the P value are as per noted.). Created in BioRender. Shi, B. (2025) BioRender.com/2vjshc8. **f** Detection of lowest Asp/PDPA-NP@ABA concentrations matching extended longevity under drought to pristine ABA at 20 d post water withdrawal, and their median survival rate, calibrated against MS, $n = 3$ biological replicates, each replicate is the mean increased median survival in comparison to that of MS treated controls (Supplementary Fig. 6j) of 24 plants. Data are presented as mean values ± SEM. Significant differences were determined using Turkey's one-way multiple comparison ANOVA test. **g** Soybean plants (15 d-old) longevity and **h** their corresponding phenotypes after a single spray with Asp/PDPA-NP@ABA versus pristine ABA at an equivalent concentration of 10 µM. Source data are provided as a Source Data file.

decomposition, and catabolism, especially in edible tissues (seed, fruit) along with monitoring impacts on the soil biome.

The Asp/PDPA-NP vehicle could also extend to other applications[44]. The chemical structure of PDPA equips this vehicle with the potential to load and deliver other hydrophobic molecules (i.e., insecticide, fertilizers or growth agents) or through electric interactions (i.e., DNA, RNA or protein) to deliver biomolecules.

A remaining question of our studies lies in the underlying regulation of the cell wall loosening by our nanocarriers. Unfortunately, this research area is still largely unknown yet is key for developing any *in planta* delivery system for plant biotechnology and crop engineering. We have indeed confirmed a temporal upregulation of cell wall remodelling genes, but as we indicated, a large majority of cell wall remodelling regulation is post-translational, and yet no known regulators offer any further explanations of how to associate our nanoparticle to cell wall remodelling. Our discover of cell wall remodelling in the presence of our nanoparticles may in fact offer a window for further investigation and we are continuing this discovery. In addition to this, how the nanoparticle interacts with the seed coat is worth pursuing in the future.

Methods

Materials

All chemicals used in this study were purchased from Sigma-Aldrich (China) unless otherwise specified. HO-PEG_{5000}-NH_2 was obtained from Ponsure Biological (China), and MeO-PEG-NH_2 was purchased from

JenKem Technology. DPA was supplied by Aladdin Reagent Co., Ltd. (Shanghai, China), and ABA was purchased from Sangon Biotech Co., Ltd. (Shanghai, China). The following staining agents were used: DiO (Yeasen, China), fluorescein-5-maleimide (MedChemExpress, Monmouth Junction, NJ, USA), and calcofluor white (MedChemExpress).

Nanoparticle characterization

^{1}H NMR

^{1}H nuclear magnetic resonance spectra were recorded on AVANCE III HD 300 MHz (Bruker, Switzerland).

Micelle formation and loading of cargos. Asp-PEG-PDPA was dissolved in tetrahydrofuran (1 mg/200 µL) with cargo (DiO dissolved in DMSO at 5 mg/mL; ABA dissolved in ethanol at 5 mg/mL), dropped in swirling aqueous solution at room temperature in a fume hood for 3 h. Thereafter, the self-assembled micellar nanoparticle solution was pelleted by ultracentrifuging 3 × 8 min at 4 °C, 3600 rpm, 1700 × *g* (Millipore ultra-4 3 K) with any unloaded cargo drug removed by decanting the flow-through. Total volume was maintained at 1 mL for each run using ddH_2O. Pellets of Asp/PDPA-NP@DiO/ABA or PDPA-NP@DiO/ABA were stored at 4 °C before use and shielded from light. The optimal encapsulation rate and particle size distribution with theoretical loading levels of DiO and ABA at 30 *w*% and 40 *w*%, respectively (Supplementary Table S2). Calculations of ABA loading were performed as per ref. 45.

Dynamic light scattering measurements. Hydrodynamic size distribution and zeta potentials of nanoparticles were determined for a polymer concentration of 1 mg/mL at 25 °C using dynamic light scattering (DLS; Zetasizer Nano-ZS, Malvern Instruments) equipped with a 633-nm He-Ne laser using backscattering detection.

Drug loading efficiency determination. For determination of DiO loading efficiency, a microplate reader was used to determine DiO concentration after ultracentrifugation set at an excitation wavelength of 484 nm and an emission wavelength of 520 nm and calculated from a standard curve.

For determination of ABA loading efficiency, the solution was filtered into a pre-chilled 1.5 mL centrifuge tube using a 0.22 µm filter head. Then HPLC was performed using acetic acid buffer (pH = 3.5) and acetonitrile as the mobile phase (*v*/*v* = 75:25) in a chromatography stainless steel column (ODS C18 250 mm × 4.6 mm), with a flow rate of 1.0 mL/min and a set time of 20 min. UV absorption detected product at 280 nm to calculate the ABA content and DLE based on a standard curve.

Before use, nanoparticles loaded with ABA, DiO or FITC were diluted with ddH_2O to specified final concentrations that corresponded with the pristine concentration of each respective molecule, to ensure identical amounts of drugs were present across treatments.

Transmission electron microscopy. A glow-discharged carbon-coated grid was used to sample the nanoparticle solution (10 µL /grid). Samples were air-dried followed by staining with 1% uranyl acetate for 7 min. Grids were then visualized with a JEM-2100 transmission electron microscope (TEM, JEOL, Japan) operated at an accelerating voltage of 200 kV.

Plant materials and growth conditions

Arabidopsis thaliana ecotype Columbia-0 (Col-0) and *ataap1* (SALK_078312), *ataap5* (SALK_041999), *ataap6* (SALK_013231), *ataap8* (SALK_081076), *atprot2* (SALK_067508) and *atlht1* (SALK_083700) mutants (Col-0 background) seeds were purchased from Arashare.

In a laminar flow cabinet and shielded from light, seeds were washed once with ddH_2O, then soaked in 75% ethanol for 1 min and washed with ddH_2O, followed by soaking in 2% sodium hypochlorite solution for 15 min and finally rinsed with ddH_2O for 6 times. Sterilised Arabidopsis seeds were stored at 4 °C. Soybean and maize seeds were airdried and stored at 4 °C.

Primers for genotyping of these mutants are listed in Supplementary Table S1.

Soybean ecotype Williams 82 (Ws82) were grown in an environmental-controlled growth chamber at 26 °C/22 °C and a 16-h light/8-h dark photoperiod and cared for as previously described[45].

Maize (*Zea mays* ssp. *mays* var. B73 -329) were grown in an environmental controlled growth chamber at 25 °C/22 °C and a 16-h light/8-h dark photoperiod[46] until 10-week-old. After application of a foliar spray, the potted plants were transferred to an outdoor growth facility with a mechanically-operated rain shelter.

Loading of nanoparticle vehicles into plants (seed germination, foliar spray application and root uptake)

For germination assays, Arabidopsis seeds were grown on ½ MS (Murashige and Skoog) liquid medium containing 1.5% sucrose at pH 6.7 in an environmental controlled growth chamber at 22 °C light/ 19.8 °C dark with a photosynthetically active radiation of 75 µmol m^{-2} s^{-1} and a 16-h light/8-h dark photoperiod. ABA or different nanoparticles were added in the liquid ½ MS medium at an equivalent amount of free ABA before seed culturing. Maize seed germination assays were performed with identical processes with the exception of culturing in ddH_2O.

For drought resistance and foliar uptake assays, sterilized seeds were germinated in ½ MS solid medium containing 1.5% sucrose at pH 5.8 in an environmental controlled growth chamber (see above) before being transplanted into soil-growth conditions (soil/vermiculite = 3:1 *w*/*w*) at 10 d. The potted plants were then transferred to growth chambers set at an 8-h light/16-h dark photoperiod. Each pot had identical amounts of water/soil (300% humidity = (water + soil)/soil (*w*/*w*)), before water withholding was initiated. Arabidopsis (wildtype or mutant) plants of identical size were foliar sprayed before being subjected to specified water withholding conditions. Foliar applications were performed with a a standard mist sprayer which dispenses precisely 60 µL of liquid/spray in which the entire mature leaf surface was exposed/plant. Equivalent concentrations of free DiO (31.8 µM), ABA (specified for each experiment) or nanoparticles loaded DiO/ABA or FITC-tagged nanoparticles were applied for each experiment. Sprayed plants were then covered with a transparent lid for 36 h to allow leaves absorb the treatment content. Pot position was changed every second day to minimize effects of any environmental gradients.

Soybean (five-week-old) and maize (3 mature leaf stage) seedlings were foliar sprayed at equivalent specified concentrations of ABA or nanoparticles before being subjected to specified water withholding conditions. Each pot was supplied with identical amounts of water/soil (300% humidity = (water + soil)/soil (*w*/*w*)), before water withholding was initiated.

Each single spray covered the entire adaxial surface of the treated leaves of all species.

For root observations, five-day-old Arabidopsis and three-day soybean or maize seedlings, germinated in liquid medium, were transferred to a culture medium containing DiO or nanoparticle loaded DiO at 31.8 µM or FITC-tagged nanoparticles for designated time points at 22 °C while shielded from the light before confocal imaging. For clathrin mediated endocytosis testing, five-day-old Arabidopsis seedlings were incubated in 300 µL ½ MS medium using 24-well plate with or without Asp/PDPA-NP@DiO with DiO at 31.8 µM for 4 or 6 h at 22 °C while shielded from the light before confocal imaging. In Tyra23 (Aladdin, China) treated groups, seedlings were pre-treated by incubation with 50 µM TyrA23 prepared in ½ MS medium for 30 min at 22 °C while shielded from the light. Tyra23 at 50 µM was also added into the nanoparticles solution during nanoparticle incubation. Confocal imaging of roots was performed on the primary roots tips.

Plant phenotype evaluation

Plant longevity to drought was tracked from water being withheld to plant death, and medium survival (time elapse when half of the treated plants are dead) is calculated accordingly.

Survival rate determination was based on a common method[46] whereby, following a specified drought period, the plants were re-watered and those that recovered were expressed as a percentage of the total population.

Confocal microscopy imaging

The confocal laser scanning microscopy images were taken on a Zeiss Confocal Microscope system (Zeiss 880).

Protoplast samples used for confocal imaging were isolated, followed by incubation with nanoparticles for 4 h in W5 medium before being washed with W5 buffer for 3 × 3 min and mounted on glass slides with W5 medium.

For leaves imaging, leaves were collected from plants in growth chambers at specified time points post spray. Before imaging, all leaves were rinsed with ddH_2O three times and then leaf segments with no large veins were mounted on slides for observation in 50% glycerol. For calcofluor white staining, leaves post spray were harvested and rinsed with ddH_2O for 3 × 10 s followed by staining with 0.1% calcofluor white (Merck) for 30 min and then rinse with ddH_2O for 3 × 10 s before mounting in 50% glycerol.

For root observations, all seedlings were rinsed in ½ MS medium and mounted in 50% glycerol on glass slides before confocal imaging.

Penetration depth tool of Zen (v2.0) was used to record the deepest penetration by the DiO signal in Arabidopsis leaves. Excitation and emission wavelengths used were: Chloroplast: Excitation 488 nm; Emission: 633 nm; FITC: Excitation 488 nm; Emission: 525 nm; DiO: Excitation 483 nm; Emission: 501 nm.

Co-localisation estimation was performed with Zen (v2.0), averaged Pearson's colocalization coefficient (r) and Manders' correlation coefficient calculated based on 3 biological replicates with 10 measurements per replicate.

Protoplast isolation

The protoplast isolation followed the protocol described by ref. 47. In short, fully-expanded leaves were collected from four-week-old wild-type Columbio-0 *A. thaliana*, and cut into 0.5 mm wide strips with a razor blade (about 10 pieces). The leaf segments were transferred to 3 mL of cell wall degradation medium (pH = 5.7, 1.5% (w/v) cellulase and 0.4% (w/v) macerozyme (Yakult, Japan)) in a six-well plate and shaken (30–40 rpm) for 3 h at 22 °C while avoiding exposure to light. Thereafter, 3 mL of a pre-cooled W5 solution (pH = 5.7) was added and shaken for 5 min to release protoplasts. Following confirming protoplast intactness by light microscopy, the protoplast suspension was filtered through 22 μm filter to remove cell debris and a protoplast pellet collected by centrifuging for 2 min at 100 g. To wash the protoplasts, the centrifugation step was repeated three times while resuspending the pellet each time in 10 mL of W5 solution.

Protoplasts were observed 20 h post in vitro culture with Asp/PDPA-NP@DiO dispensed in W5 solution for 4 h at 22 °C while avoiding the light.

ABA extraction and content determination from isolated protoplasts and accompanying extracellular matrix

Protoplasts and extracellular matrix samples collection. All leaves of each treatment group were collected from 23-day-old wild-type *A. thaliana* plants 24 h post spray with a concentration of 10 μM ABA or equivalent when loaded in nanoparticles. Three biological replicates were collected with 24 plants for each replicate. Before collection, all leaves were rinsed with ddH_2O for three times to remove any residues to exclude interference with the experiment, and the leaves were gently blotted with paper towel to prevent dilution of the enzyme digest for harvesting protoplasts. All leaves were cut, placed in the enzyme solution (pH = 5.7), and shaken at 30–40 rpm for 3 h. All liquids were collected and centrifuged followed by collection of all protoplasts deposited at the bottom of centrifuge tubes, and all supernatants were also collected and to be stored individually before quick-frozen in liquid nitrogen. In each replicate, 1 g protoplasts were isolated. Quality of isolated protoplasts were examined under light microscopes to ensure > 95% of intact cells in each isolation. All the supernatants and residues were combined and freeze-dried for each replicate of each treatment, stored at −80 °C, and the ABA contents of each replicate of different treatment were determined by LC-MS as described in the following section.

In addition, the washing steps before the enzyme digestion should have removed all small molecular residue, hinting that the PDPA/NP@ABA may have bounded to the cell wall.

Quantification of ABA by UPLC-ESI-MS/MS. ABA quantification was performed in external resourced lab using a UPLC-ESI-MS/MS system adapted from previously published methods[48]. In short, the analysis was carried out on a Waters Acquity I-Class UHPLC system (Waters, USA) coupled to a Qtrap 4000 triple quadrupole mass spectrometer equipped with an electrospray ionization (ESI) source (AB Sciex, USA). Samples were extracted in 80% methanol and filtered through a 0.22 μm nylon micromembrane prior to injection. Chromatographic separation was achieved on an Acquity UHPLC BEH C18 column (2.1 × 100 mm, 1.7 μm) maintained at 40 °C. The mobile phase consisted of solvent A (acetonitrile) and solvent B (water with 0.1% formic acid, v/v). A gradient elution program was applied as follows: 0–0.5 min, 5% A; 0.5–3.0 min, 5–60% A; 3.0–3.5 min, 60–95% A; 3.5–5.0 min, 95% A; 5.0–5.1 min, 95–5% A; and 5.1–7.0 min, 5% A. The flow rate was 0.4 mL/min and the injection volume was 1.0 μL.

Mass spectrometric detection was performed in negative ion mode using multiple reaction monitoring. The optimized MS parameters were as follows: curtain gas (CUR), 40 psi; ion spray voltage (IS), −4500 V; temperature (TEM), 550 °C; ion source gas 1 (GS1), 55 psi; ion source gas 2 (GS2), 55 psi; declustering potential (DP), −85 V; entrance potential (EP), −10 V; collision energy (CE), −14 V; and cell exit potential, −9 V. The limit of detection and limit of quantification were defined as signal-to-noise (S/N) ratios of 3 and 10, respectively. Data were acquired and processed using SCIEX MultiQuant software. Each sample was analyzed in technical triplicates to ensure reproducibility.

Leaf temperature detection and quantification

Leaf temperature was captured with an infrared imager (FLIR T640) before and after spray and analysed by first converting the infrared photographs to binary (black and white) images using Photoshop CS6. Free-hand selection tool of Fiji software (https://fiji.sc/) was used to select specified leaves in which mean pixel intensity of entire leaf area temperature was determined (Mean gray value option). A total of 24 plants (two mature leaves per plant) were analysed for each treatment. Due to the fact that plants exhibit variation of foliar temperature between day and night, changes in calculated temperature were normalized against MS treatment.

Quantitative real-time PCR and RNA Sequencing

Total RNAs were extracted from three-week-old Arabidopsis leaves sprayed with ABA or nanoparticles at specified time points using MiniBEST Plant RNA Extraction Kit (TaKaRa). Reverse transcriptions were performed following instructions of PrimeScript™ RT reagent Kit with gDNA Eraser (Perfect Real Time). All qRT-PCR assays were conducted following protocols of the Amp™ SYBR® Green qPCR Mix (Low ROX) with a Roche LightCycler 480 RT-PCR System (95 °C × 15 s, 60 °C × 60 s, 40 cycles). All transcripts expression levels were normalized against the house-keeping gene *A. thaliana ACTIN 2* (*AtACTIN2*). Standard curve thresholds were set to equivalent values for all

genes. Expression levels were calculated based on comparative C_t method ($2^{-\Delta\Delta Ct}$). Each assay includes three biological replicates per sample. Primers used in all qRT-PCR assays are exhibited in Supplementary Table S1.

Total RNA samples were extracted (see above) at specified time points and sent to Novogene Co., Ltd. (Beijing) for RNA Sequencing (RNA-Seq). The transcriptome data are available on NCBI. Differentially expressed genes (DEGs) were defined as exhibiting a differential expression of twofold or more ($p < 0.05$).

Statistics and data analysis

Statistical differences between means were processed and analysed with GraphPad Prism (V) software and assessed using Turkey's one-way ANOVA multiple comparison test unless otherwise noted. Three biological replicates and two technical replicates were performed for each treatment in qPCR analyses. Biological/technical replications for all other experiments are as per denoted.

Reporting summary

Further information on research design is available in the Nature Portfolio Reporting Summary linked to this article.

Data availability

Source data are provided with this paper. The sequencing data generated in this study have been deposited into NCBI under the project accession number PRJNA1072859. The raw data supporting the finding from this study are provided in the Source Data file. Source data are provided with this paper.

References

1. Bailey-Serres, J., Parker, J. E., Ainsworth, E. A., Oldroyd, G. E. D. & Schroeder, J. I. Genetic strategies for improving crop yields. *Nature* **575**, 109–118 (2019).
2. Gao, C. Genome engineering for crop improvement and future agriculture. *Cell* **184**, 1621–1635 (2021).
3. Poon, W., Kingston, B. R., Ouyang, B., Ngo, W. & Chan, W. C. W. A framework for designing delivery systems. *Nat. Nanotechnol.* **15**, 819–829 (2020).
4. Mao Y., Botella J. R., Liu Y. & Zhu J.-K. Gene editing in plants– progress and challenges. *Nat. Sci. Rev.* **6**, 421–437 (2019).
5. Park, H., Otte, A. & Park, K. Evolution of drug delivery systems: from 1950 to 2020 and beyond. *J. Control Release* **342**, 53–65 (2022).
6. Cosgrove, D. J. Re-constructing our models of cellulose and primary cell wall assembly. *Curr. Opin. Plant Biol.* **22**, 122–131 (2014).
7. Carpita, N., Sabularse, D., Montezinos, D. & Delmer, D. P. Determination of the pore size of cell walls of living plant cells. *Science* **205**, 1144–1147 (1979).
8. Avellan, A. et al. Nanoparticle size and coating chemistry control foliar uptake pathways, translocation, and leaf-to-rhizosphere transport in wheat. *ACS Nano* **13**, 5291–5305 (2019).
9. Zhang, H. et al. Nanoparticle cellular internalization is not required for RNA delivery to mature plant leaves. *Nat. Nanotechnol.* **17**, 197–205 (2022).
10. Spielman-Sun, E. et al. Nanoparticle surface charge influences translocation and leaf distribution in vascular plants with contrasting anatomy. *Environ. Sci. Nano* **6**, 2508–2519 (2019).
11. Roell, M.-S. A novel Trojan horse for molecule delivery into plants. *Plant Physiol.* **184**, 548–549 (2020).
12. Santana, I., Wu, H., Hu, P. & Giraldo, J. P. Targeted delivery of nanomaterials with chemical cargoes in plants enabled by a biorecognition motif. *Nat. Commun.* **11**, 2045 (2020).
13. Demirer, G. S. et al. High aspect ratio nanomaterials enable delivery of functional genetic material without DNA integration in mature plants. *Nat. Nanotechnol.* **14**, 456–464 (2019).
14. Zhang, H. et al. DNA nanostructures coordinate gene silencing in mature plants. *Proc. Natl. Acad. Sci. USA* **116**, 7543–7548 (2019).
15. Jeon, S.-J. et al. Targeted delivery of sucrose-coated nanocarriers with chemical cargoes to the plant vasculature enhances long-distance translocation. *Small* **20**, 2304588 (2022).
16. Liu, X. et al. Engineering blood-brain barrier-permeable and tumor cell-ingestible pro-proteins for glioblastoma treatment. *Sci. China Chem.* **66**, 2634–2644 (2023).
17. Vig, B. S., Huttunen, K. M., Laine, K. & Rautio, J. Amino acids as promoieties in prodrug design and development. *Adv. Drug Deliv. Rev.* **65**, 1370–1385 (2013).
18. Tegeder, M. Transporters for amino acids in plant cells: some functions and many unknowns. *Curr. Opin. Plant Biol.* **15**, 315–321 (2012).
19. Lee, Y.-H. et al. AAP1 transports uncharged amino acids into roots of Arabidopsis. *Plant J.* **50**, 305–319 (2007).
20. Svennerstam, H., Ganeteg, U., Bellini, C. & Näsholm, T. Comprehensive screening of Arabidopsis mutants suggests the lysine histidine transporter 1 to be involved in plant uptake of amino acids. *Plant Physiol.* **143**, 1853–1860 (2007).
21. Hirner, A. et al. Arabidopsis LHT1 is a high-affinity transporter for cellular amino acid uptake in both root epidermis and leaf mesophyll. *Plant Cell* **18**, 1931–1946 (2006).
22. Tegeder, M. & Rentsch, D. Uptake and partitioning of amino acids and peptides. *Mol. Plant* **3**, 997–1011 (2010).
23. Ren, Z. et al. Overexpression of *AtAAP1* increased the uptake of an alanine-chlorantraniliprole conjugate in *Arabidopsis thaliana*. *Environ. Sci. Pollut. Res.* **26**, 36680–36687 (2019).
24. Ortiz-Lopez, A., Chang, H. C. & Bush, D. R. Amino acid transporters in plants. *Biochim. Biophys. Acta (BBA) - Biomembranes* **1465**, 275–280 (2000).
25. Chimpan, C. & Sipos, M. Anatomy of the vegetative organs of *Tradescantia pallida purpurea*. *Biharean Biol.* **3**, 1–4 (2009).
26. Liu, X. et al. Auxin controls seed dormancy through stimulation of abscisic acid signaling by inducing ARF-mediated *ABI3* activation in *Arabidopsis*. *Proc. Natl. Acad. Sci. USA* **110**, 15485–15490 (2013).
27. Shu, K., Liu, X. -d, Xie, Q. & He, Z. -h Two faces of one seed: hormonal regulation of dormancy and germination. *Mol. Plant* **9**, 34–45 (2016).
28. Fukuda, H., Kuramochi, H., Shibuta, Y. & Ichiki, T. Analysis of Brownian motion trajectories of non-spherical nanoparticles using deep learning. *APL Mach. Learn.* **1**, 046104 (2023).
29. Minoura, I., Katayama, E., Sekimoto, K. & Muto, E. One-dimensional Brownian motion of charged nanoparticles along microtubules: a model system for weak binding interactions. *Biophys. J.* **98**, 1589–1597 (2010).
30. Shen, J. et al. Organelle pH in the Arabidopsis endomembrane system. *Mol. Plant* **6**, 1419–1437 (2013).
31. McKay, D. W. et al. Plant trans-Golgi network/early endosome pH regulation requires cation chloride cotransporter (CCC1). *eLife* **11**, e70701 (2022).
32. Rayle, D. L. & Cleland, R. E. Evidence that auxin-induced growth of soybean hypocotyls involves proton excretion. *Plant Physiol.* **66**, 433–437 (1980).
33. Cao, M. et al. An ABA-mimicking ligand that reduces water loss and promotes drought resistance in plants. *Cell Res.* **23**, 1043–1054 (2013).
34. Cao, M.-J. et al. Combining chemical and genetic approaches to increase drought resistance in plants. *Nat. Commun.* **8**, 1183 (2017).
35. Zhu, Y. et al. CDK8 is associated with RAP2. 6 and SnRK2. 6 and positively modulates abscisic acid signaling and drought response in Arabidopsis. *New Phytol.* **228**, 1573–1590 (2020).

36. Murphy, A. S., Bandyopadhyay, A., Holstein, S. E. & Peer, W. A. Endocytotic cycling of PM proteins. *Annu. Rev. Plant Biol.* **56**, 221–251 (2005).
37. Zhou, Y. et al. Blood-brain barrier–penetrating siRNA nanomedicine for Alzheimer's disease therapy. *Sci. Adv.* **6**, eabc7031 (2020).
38. Dejonghe, W. et al. Disruption of endocytosis through chemical inhibition of clathrin heavy chain function. *Nat. Chem. Biol.* **15**, 641–649 (2019).
39. Jeannette, E. et al. Induction of *RAB18* gene expression and activation of K^+ outward rectifying channels depend on an extracellular perception of ABA in *Arabidopsis thaliana* suspension cells. *Plant J.* **18**, 13–22 (1999).
40. Gupta, A., Rico-Medina, A. & Caño-Delgado, A. I. The physiology of plant responses to drought. *Science* **368**, 266–269 (2020).
41. Tai, L. et al. Pre-harvest sprouting in cereals: genetic and biochemical mechanisms. *J. Exp. Bot.* **72**, 2857–2876 (2021).
42. Yu, S.-M., Lo, S.-F. & Ho, T.-H. D. Sink communication: regulated by hormone, nutrient, and stress cross-signaling. *Trends Plant Sci.* **20**, 844–857 (2015).
43. Tester, M. & Langridge, P. Breeding technologies to increase crop production in a changing world. *Science* **327**, 818–822 (2010).
44. Savage, N. Improving crop resilience with nanoparticles. *Nature* **608**, S16–S17 (2022).
45. Sun, H. et al. Biodegradable micelles with sheddable poly(ethylene glycol) shells for triggered intracellular release of doxorubicin. *Biomaterials* **30**, 6358–6366 (2009).
46. Nuccio, M. L. et al. Expression of trehalose-6-phosphate phosphatase in maize ears improves yield in well-watered and drought conditions. *Nat. Biotechnol.* **33**, 862–869 (2015).
47. Yoo, S. D., Cho, Y. H. & Sheen, J. Arabidopsis mesophyll protoplasts: a versatile cell system for transient gene expression analysis. *Nat. Protoc.* **2**, 1565–1572 (2007).
48. Zhang, Z. et al. High-performance liquid chromatographic quantification of the plant hormone abscisic acid at ppb levels in plant samples after a single immunoaffinity column cleanup. *J. Agric. Food Chem.* **72**, 11794–11803 (2024).

Acknowledgements

We thank A/Prof. Si Shen of China Agricultural University for inspiring discussion of maize growth and phenotyping, and Prof. Tian Zhang of Henan University for supportive discussion of cell wall remodelling and permeability. This work was supported by Henan Natural Science Foundation (232300421044, M.Z.), the Program of Technology Innovation Team of the Colleges and Universities of Henan Province (25IRTSTHN032, M.Z.), National Natural Science Foundation of China (NSFC 32001432, X.X.), the China National Postdoctoral Program for Innovative Talent, China Postdoctoral Science Foundation (Grant No. BX20240103, Y.Liu), the Natural Science Foundation of Henan (Grant No. 242300420457, Y.Liu), and Henan University Double First-Class Foundation.

Author contributions

X.X, J.D., A.L. contributed equally to this work. Conceptualization: X.X., Y.Zhu, Y.Liu, S.S., J.P., C.O., M.Z. B.S. Methodology: X.X., J.D., Y.Zhu, Y.Zou, A.S., Y.Lu, M.Z., C.P.S. Investigation: A.L., Y.W., L.X., Z.J., J.W. Visualization: A.L., Y.W., L.X., Z.J., J.W. Project administration: X.X., Y.Liu, Y.Zhu, S.S., L.W., Y.Lu, X.W., J.P., C.O., M.Z., C.P.S., B.S. Supervision: M.Z., C.P.S., B.S. Writing–original draft: X.X. Writing–review & editing: X.X., Y.Liu, Y.Zhu, Y.Zou, Y.Lu, S.S., L.W., X.W., J.P., C.O., M.Z., C.P.S., B.S.

Competing interests

The authors declare the following competing interests: X.X. filed a patent application based on this study to the State Intellectual Property Office of China and applied the Patent Cooperation Treaty. The other authors declare no competing interests.

Additional information

Supplementary information The online version contains supplementary material available at https://doi.org/10.1038/s41467-025-60829-8.

Correspondence and requests for materials should be addressed to Meng Zheng, Chun-Peng Song or Bingyang Shi.

Peer review information *Nature Communications* thanks the anonymous reviewer(s) for their contribution to the peer review of this work. [A peer review file is available].